Title

Adipose depot-specific effects of ileal interposition surgery in UCD-T2D rats: unexpected implications for obesity and diabetes.

Journal

Biochemical Journal, 475(3)

ISSN

0264-6021

Authors

Hung, Connie
Bronec, Casey
Napoli, Eleonora
et al.

Publication Date

2018-02-14

DOI

10.1042/bcj20170899

Peer reviewed

Biochemical Journal (2018) **475** 649–662
https://doi.org/10.1042/BCJ20170899

Research Article

Adipose depot-specific effects of ileal interposition surgery in UCD-T2D rats: unexpected implications for obesity and diabetes

Connie Hung[1], Casey Bronec[1], Eleonora Napoli[1], James Graham[2], Kimber L. Stanhope[1,2], Ilaria Marsilio[1,3], Maria Cecilia Giron[3], Peter J. Havel[1,2] and Cecilia Giulivi[1,4]

[1]Department of Molecular Biosciences, School of Veterinary Medicine, University of California, Davis, CA 95616, U.S.A.; [2]Department of Nutrition, University of California, Davis, CA 95616, U.S.A.; [3]Department of Pharmaceutical and Pharmacological Sciences, Pharmacology Building, University of Padova, Largo Meneghetti 2, 35131 Padova, Italy; [4]Medical Investigations of Neurodevelopmental Disorders (M. I. N. D.) Institute, University of California, Davis, CA 95817, U.S.A.

Correspondence: Cecilia Giulivi (cgiulivi@ucdavis.edu)

Ileal interposition (IT) surgery delays the onset of diabetes in a rat model of type-2 diabetes (UCD-T2DM). Here, to gain a deeper understanding of the molecular events underlying the effects of IT surgery, we examined the changes in the proteome of four white adipose depots (retroperitoneal, mesenteric, inguinal, and epididymal) and plasma-free fatty acid profile in pre-diabetic rats 1.5 months following IT or sham surgery. The IT-mediated changes were exerted mainly in mesenteric fat and spanned from delayed adipocyte maturation to a neuroendocrine remodeling. Conversely, inguinal, retroperitoneal, and epididymal depots showed opposite trends consistent with increased adipocyte maturation and adipogenesis development prior to overt signs of diabetes, probably orchestrated by peroxisome proliferator-activated receptor gamma signaling and higher plasma *n*-6/*n*-3 free fatty acid ratios. The resulting scenario suggests a targeted use of surgical strategies that seek to delay or improve diabetes in order to manipulate adipose depot-specific responses to maximize the duration and beneficial effects of the surgery.

Introduction

The unquestioned role of obesity-induced insulin resistance in the pathogenesis of type-2 diabetes mellitus (T2DM), a metabolic disease estimated to affect more than 400 million people worldwide [1], is an important indication of the strong link between dysregulation of cellular energy metabolism and the development of T2DM.

Ileal interposition (IT) surgery, by delivering incompletely digested nutrients as well as biliary and pancreatic secretions to the distal intestinal (ileal) mucosa [2], mimics one important component of gastric bypass surgery, which has been shown to improve glucose homeostasis and reverse insulin resistance and T2DM [3–5]. In a previous study, we reported that IT surgery delayed diabetes onset in UCD-T2DM rats [6], increased circulating bile (cholic) acid levels, decreased endoplasmic reticulum (ER) stress, and inflammation [7], improved insulin signaling (in fat, liver, skeletal muscle, and pancreas), and enhanced glucose-stimulated insulin secretion and preservation of islet integrity and β-cell mass. However, as of today, an integrated view of the effects of IT surgery on fat depots is still missing.

Considering the obesity epidemic, there is substantial interest in the biology of adipose tissue. While increased visceral fat mass is associated with a higher risk of metabolic dysfunction, increased subcutaneous white adipose tissue (WAT) is not [8,9]. There are six major internal fat depots: perirenal, gonadal, epicardial, retroperitoneal, omental, and mesenteric. Interestingly, unlike other pads, the blood supply of the mesenteric depot reaches liver directly through the portal circulation, which according to the Bjorntorp's hypothesis [10], underlies the mesenteric depot's direct involvement in

Received: 27 November 2017
Revised: 2 January 2018
Accepted: 7 January 2018

Accepted Manuscript online: 10 January 2018
Version of Record published: 14 February 2018

Biochemical Journal (2018) 475 649–662
https://doi.org/10.1042/BCJ20170899

the pathology of cardiovascular disease and T2DM. Given that the expansion of the visceral WAT is closely associated with human diseases such as T2DM, fatty liver disease, and cardiovascular disease, it is likely that the mesenteric depot is directly relevant to the pathophysiology of metabolic disease in humans. Yet, this particular depot is often excluded from analyses.

In the present study, we applied proteomic analyses to investigate the effects of IT surgery on the metabolism of four WAT depots: one subcutaneous (SC; inguinal), and three intra-abdominal (IA), of which one visceral and intraperitoneal (mesenteric, associated with internal digestive organs and with venous drainage into the portal system) and two non-visceral (retroperitoneal and epididymal-associated with the reproductive organs). These studies were complemented and extended by plasma-free fatty acid (FFA) profile. We employed UCD-T2DM rats, as a biological model of T2DM, which exhibit a pathophysiology representative of the clinical manifestations observed in humans, i.e. insulin resistance with inadequate insulin compensation and intact leptin signaling compared with most other rodent models of T2DM [11].

While the understanding of the molecular regulation of adipogenesis is mainly based on information obtained thus far from transcriptome data [12], our approach (the use of proteomics applied to the study of whole fat depots, as opposed to isolated adipocytes) should circumvent the less-than-robust (and gene-specific [13]) correlations between mRNA levels and protein expression [14] that occurs as a result of translational controls exerted by transcription factors, microRNAs, and epigenetic factors, concurrently taking into account metabolic differences between fat depots *in vivo*.

Materials and methods

Chemicals and biochemicals

Acetone, EDTA, EGTA, sodium succinate, mannitol, sucrose, and HEPES were all purchased from Sigma (St. Louis, MO). Tris–HCl, glycine, sodium chloride, and potassium chloride were purchased from Fisher (Pittsburg, PA). Bovine serum albumin (fatty acid free) was obtained from MP Biomedicals. All other reagents were of analytical or higher grade.

Animals

Male UCD-T2DM rats were individually housed on a 14–10 h light–dark cycle in wire cages in the animal facility of the Department of Nutrition (University of California, Davis). For the present study, only male mice were used to avoid confounding effects arising from sex hormonal cycles. Non-fasting glucose levels were assessed weekly between 14:00 and 16:00 h by a glucometer (One-Touch Ultra, Life Scan, Milpitas, CA), with diabetes onset defined as testing a non-fasted blood glucose value >200 mg/dl for two consecutive weeks. At 2 months of age, rats received either IT surgery or sham (sham) surgery. Evaluation of hormone and plasma metabolites was performed as described before [6]. The two groups, IT ($n = 10$) and sham ($n = 9$), were killed 1.5 m post-surgery for tissue collection. All experimental protocols were approved by the UCD Institutional Animal Care and Use Committee and followed the NIH guidelines.

Surgery

The procedure for IT surgery was performed as described in detail in Cummings et al. [15]. After cutting a midline abdominal incision, a segment of ileum (∼10 cm) ∼5–10 cm proximal to the ileocecal valve was transected. The ends of the ileum were anastomosed using a 7-0 PDS suture (Ethicon). The isolated ileal transection was then transposed 5–10 cm distal to the ligament of Treitz with its vasculature supply. Rats that underwent the sham surgery were subjected to the same protocol, but transections made in the identical location were anastomosed in their original position without translocation.

Tissue collection

At 1.5 months after either IT surgery or sham surgery (when the rats were 3.5 ± 0.5 months old), they were euthanized with an overdose of pentobarbital (200 mg/kg, i.p.). The four fat depots (retroperitoneal, mesenteric, inguinal, and epididymal), excluding corresponding lymph nodes and blood vessels, were collected and weighted. An aliquot was set aside for fat content (see below) and the remaining aliquots were immediately stored at −80°C. The retroperitoneal depot was dissected from behind the kidney and along the dorsal portion of the abdomen excluding the WAT around the kidney (considered as 'perirenal'). For the evaluation of fat content, each depot was extracted with Folch extraction procedure, the extracted organic layer was dried under

nitrogen, and the final dry residue was weighted as described before [16]. Data were normalized *per* rat. For adipocyte sizing, samples were evaluated at the UCD Veterinary Medicine Teaching Hospital for a service fee. Formalin-fixed samples were embedded in paraffin, sliced into 5-μm sections, mounted, and stained with hematoxylin and eosin. Stained slides were examined under a microscope equipped with a digital camera following the approach described by Chen and Farese [17] based on the cross-sectional area of all the adipocytes present in three or more non-overlapping microscope fields. Plasma samples were collected and analyzed for FFA composition by the UCD Mass Spectrometry Facility.

Proteomics analyses

Sample preparation

Equivalent amounts of adipose tissue from 10 IT or 9 sham individual rats were pooled into either sham or IT groups. Samples were delipidated in detail as described before [18]. Pellets were subsequently diluted in buffer containing 7 M urea, 2 M thiourea, 1% (w/v) sulfobetaine-10, 3% (w/v) CHAPS, and 1.5% (v/v) protease inhibitor cocktail (Sigma, St. Louis, MO). Protein solubilization was achieved through mechanical homogenization followed by brief sonication, incubation at 35°C for 15 min, and centrifugation at 16 000***g*** for 45 min at room temperature. Protein evaluation was performed with the Pierce BCA protein assay (Thermo Scientific, Waltham, MA). Samples were submitted to the UCD Core Proteomics Facility where they were digested overnight with a trypsin to protein ratio of 1 : 30. The equivalent of 2–5 μg of protein was loaded for liquid chromatography–mass spectrometry (LC–MS/MS) analysis.

Database searching

All MS/MS samples were analyzed using X! Tandem [The GPM, thegpm.org; version TORNADO (2010.01.01.4)]. X! Tandem was set up to search the uniprot__20120523_gTmkm3 database (89576 entries), assuming the digestion by the enzyme trypsin. X! Tandem was searched with a fragment ion mass tolerance of 20 ppm and a parent ion tolerance of 1.8 Da. Deamidation of Asn and Gln, oxidation of Met and Trp, sulfone of Met, Trp oxidation to formylkynurenin, and acetylation of the N-terminus were specified in X! Tandem as variable modifications.

Criteria for protein identification

Scaffold (v. 3.00.07, Proteome Software, Inc., Portland, OR) was used to validate MS/MS-based peptide and protein identification. Peptide identification was accepted if it could be established at >80% probability by the Peptide Prophet algorithm [19]. Protein identifications were accepted if they could be established at >80.0% probability and contained at least two identified peptides. Protein probabilities were assigned by the Protein Prophet algorithm [20]. Proteins that contained similar peptides and could not be differentiated based on MS/MS analysis alone were grouped to satisfy the principles of parsimony.

Free fatty acid profile

This analysis was performed at the Mass spectrometry Facility at UC Davis and following protocol essentially described in ref. [21]. Aliquots (20 μl) of plasma from 13 sham and 12 IT animals, stored at −80°C, were thawed (10 min at 4°C), extracted, derivatized, and the metabolite abundances quantified by gas chromatography time-of-flight (GC-TOF) MS. Briefly, aliquots were extracted with 1 ml of degassed acetonitrile/isopropanol/water (3 : 3 : 2) solution at −20°C, centrifuged, the supernatants removed, and solvents evaporated to dryness under reduced pressure. To remove membrane lipids and triglycerides, dried samples were reconstituted with acetonitrile/water (1 : 1), decanted, and taken to dryness under reduced pressure. Internal standards, C8-C30 FFA methyl esters, were added to samples and derivatized with methoxyamine hydrochloride in pyridine and subsequently by *N*-methyl-*N*-(trimethylsilyl)trifluoroacetamide for trimethylsilylation of acidic protons. Derivatized samples were analyzed on an Agilent 6890/5975 MSD gas chromatograph (Santa Clara, CA) with a 30 m long, 0.25 mm i.d. DB225MS column with 0.25 μm 5% diphenyl film with an additional 10 m integrated guard column (Agilent Technologies). An aliquot (1 μl) was injected at 50°C (ramped to 225°C) in splitless mode with a 25 s splitless time. The chromatographic gradient consisted of a constant flow of 1 ml/min, ramping the oven temperature from 60°C, increased with a rate of 10°C/min with a total run time of 28.5 min. Mass spectrometry was performed using a Leco Pegasus IV time-of-flight mass spectrometer, 230°C transfer line temperature, electron ionization at −70 V, and an ion source temperature of 250°C. Mass spectra were

Biochemical Journal (2018) **475** 649–662
https://doi.org/10.1042/BCJ20170899

acquired at 1800 V detector voltage at m/z 85–500 with 17 spectra/s. Acquired spectra were further processed using the BinBase database. Detailed criteria for peak reporting included mass spectral matching, spectral purity, signal-to-noise ratio, and retention time. All entries in BinBase were matched against the Fiehn mass spectral library of 1200 authentic metabolite spectra using retention index and mass spectrum information, or the NIST11 commercial library. All samples were analyzed in one batch, and data quality and instrument performance were constantly monitored using quality control samples (National Institute of Standards and Technology). Quality controls were comprised of a mixture of standards and analyzed every 10 samples, were monitored for changes in the ratio of the analyte peak heights, and used to ensure equivalent conditions within the instrument.

Calculations of free fatty acid-derived parameters

These parameters were calculated essentially as described in ref. [22], with the following modifications. For each animal, the plasma FFA concentrations were converted to μM with appropriate standards run in parallel. The average chain length (ACL) was calculated as = (Σ [Total Cni FA] × ni) where n = carbon atom number); double bond index or DBI = (Σ [Monoenoic FA] × 1) + (Σ [Dienoic FA] × 2) + (Σ [Trienoic FA] × 3) + (Σ [Tetraenoic FA] × 4) + (Σ [Pentaenoic FA] × 5) + (Σ [Hexaenoic FA] × 6); and peroxidizability index or PI = [(0.025 × Σ [Monoenoic FA]) + (1 × Σ [Dienoic FA]) + (2 × Σ [Trienoic FA]) + (4 × [Tetraenoic FA]) + (6 × Σ [Pentaenoic FA]) + (8 × Σ [Hexaenoic FA)]. This last index takes into account that the peroxidation increases as an exponential function of the number of double bonds *per* fatty acid.

Enzymatic activities of fat depots were estimated as the product-to-precursor ratios of individual plasma FFAs [23] as follows: stearoyl-CoA desaturase = 16:1 n-7/16:0 or 18:1 n-9/18:0, elongase = 18:0/16:0 or 18:1 n-7/16:1 n-7, D5D = 20:4 n-6/20:3 n-6, D6D = 18:3 n-6/18:2 n-6, and *de novo* lipogenesis = 16:0/18:2 n-6.

Statistics

Proteomics data were analyzed with two-tailed Student's t-test with unequal variances (between IT and sham treatments) with a significance level set at $P \leq 0.05$. Proteomic analysis considered all protein peptides from the dataset that had exclusive spectrum counts of at least ±0.3 (LOG2 ratio IT/sham) and $P \leq 0.05$. The comprised list was analyzed by using Metabonalayst [24], with the statistical methods therein. FFA profile data and indices were analyzed by using Kruskal–Wallis.

Results

IT surgery decreased circulating active glucagon-like peptide-1, insulin-to-glucagon ratio, and fasting glycemia and lipidemia at 1.5 m after IT surgery

As observed before, none of the UCD-T2DM rats that underwent either IT or sham surgery developed overt diabetes at 1.5 months post-surgery. In IT-operated animals, fasting plasma glucose and triglycerides (TG) were, respectively, reduced by 11% and 21%, while fasting plasma insulin was reduced by ∼50% compared with sham-operated animals (Table 1). In addition, circulating concentrations of the total glucagon-like peptide-1 (GLP-1, insulin-secretion mediator [25]) and the active/total GLP-1 ratio were higher in IT-operated rats, whereas plasma glucagon, adiponectin, and monocyte chemoattractant protein-1 were not different between the two groups (Table 1).

Body weight did not differ between IT- and sham-operated animals, although total and depot-specific fat mass was reduced by ∼20% in IT-operated animals (Table 2), suggesting either increased lipolytic capacity or decreased recruitment and/or maturation of pre-adipocytes into adipocytes.

Proteomic profiles of WAT depots after IT surgery

The observed decreases in fat mass in IT-operated UCD-T2DM rats prompted us to take a deeper look at the intermediary metabolism of these depots by analyzing their proteome profiles.

At 1.5 months after sham or IT surgery, protein-enriched fractions from four WATs, namely epididymal, retroperitoneal, mesenteric, and inguinal, were obtained from UCD-T2DM rats. To evaluate the effects of the IT surgery, statistical analyses on the WAT proteome profiles were performed by setting the threshold for differentially expressed proteins at $|\text{LOG2 ratio IT/sham}| \geq 0.3$ and $P \leq 0.05$ (Supplementary Dataset). The number of differentially expressed proteins in each depot in response to IT surgery was as follows: epididymal

Table 1 Metabolic and endocrine outcomes at 1.5 months after IT or sham surgery

Outcome	Sham	IT	Change (%)	*P*-value
	Mean ± SEM (*n*)			
Glucose and lipids				
Non-fasting glucose (mg/dl)	128 ± 5 (16)	139 ± 4 (16)		0.115
Fasting glucose (mg/dl)	113 ± 3 (12)	101 ± 1 (11)	−11%	**0.001**
HbA_{1c} (%)	4.5 ± 0.2 (12)	4.3 ± 0.2 (12)		0.416
Fasting TG (mg/dl)	136 ± 10 (12)	108 ± 7 (12)	−21%	**0.041**
Fasting FFA (mEq/l)	0.90 ± 0.06 (12)	1.01 ± 0.03 (12)		0.137
Fasting cholesterol (mg/dl)	110 ± 3 (12)	101 ± 4 (12)		0.079
Fasting hormone concentrations				
Insulin (pM)	519 ± 34 (12)	280 ± 0.1 (12)	−47%	**<0.0001**
Glucagon (pg/ml)	58 ± 2 (12)	63 ± 7 (12)		0.076
Adiponectin (μg/ml)	5.7 ± 0.6 (12)	6.3 ± 0.2 (12)		0.392
Total GLP-1 (pg/ml)	5 ± 1 (12)	14 ± 2 (12)	180%	**0.002**
Active GLP-1 (pg/ml)	3.8 ± 0.4 (12)	5.0 ± 0.4 (12)		0.059
Active/total GLP-1	1.1 ± 0.3 (12)	0.5 ± 0.1 (12)	−56%	**0.049**
MCP-1 (pg/ml)	1014 ± 39 (6)	945 ± 50 (6)		0.290

n = number of animals; values in bold indicate $P \leq 0.05$. Abbreviations: FFA: free fatty acids; GLP-1: glucagon-like peptide-1; Hb: hemoglobin; MCP-1: monocyte chemoattractant protein-1; TG: triglycerides.

267; retroperitoneal 141; mesenteric 111; and inguinal 80. Upon IT surgery, epididymal fat also had the highest number of uniquely (not shared by any other depot) differentially expressed proteins ($n = 144$), followed by retroperitoneal ($n = 42$), mesenteric ($n = 28$) and inguinal with only 22. Of note, while the higher number of unique proteins identified in the epididymal depot might suggest that this tissue was the one that responded most robustly to IT surgery, the number of unique proteins *per* depot was proportional to the total number of proteins for each depot (number of unique proteins $= 5.7 + 0.002 \times [\text{number of total proteins}]^{1.98}$; $R^2 = 0.998$,

Table 2 Adipose depot weights in age-matched sham and IT UCD-T2DM rats at 1.5 months after surgery

Fat depot	IT/sham fat mass (mean ± SEM) (g)	*P*-value*
Intra-abdominal		
Non-visceral		
Epididymal	0.8 ± 0.3	**0.018**
Retroperitoneal	0.7 ± 0.3	**0.012**
Visceral		
Mesenteric	0.8 ± 0.3	0.059
Subcutaneous		
Inguinal	0.8 ± 0.3	0.081
Total adipose tissue	0.8 ± 0.2	**0.002**

**P*-values obtained with one-tailed Student's *t*-test. Values in bold indicate $P \leq 0.05$. Each group consisted of 12 animals. Depot weights in sham-treated animals were 6.0 ± 0.5, 9.4 ± 0.8, 7.5 ± 0.7, 34 ± 2, and 57 ± 3 for epididymal, retroperitoneal, mesenteric, subcutaneous, and total, respectively (mean ± SEM in g).

Biochemical Journal (2018) **475** 649–662
https://doi.org/10.1042/BCJ20170899

Table 3 Fat depot wet weights, protein content, and number of proteins per depot in UCD-T2DM upon IT surgery

Fat depot	Fat content (g) *per* 100 g of body weight (mean ± SEM)	Protein content (mg) *per* g fat (mean ± SEM)	Number of proteins *per* depot
Intra-abdominal			
Epididymal	1.4 ± 0.1	5.1 ± 0.3	267
Retroperitoneal	1.9 ± 0.1	5.2 ± 0.4	141
Mesenteric	1.6 ± 0.1	10 ± 1	111
Subcutaneous			
Inguinal	7.2 ± 0.6	4.5 ± 0.3	80

Each group consisted of 12 animals at 1.5 months after surgery.

$P < 0.01$). Moreover, the number of proteins with differential abundance in response to IT surgery *per* fat depot did not show any correlation with either fat or protein contents (Table 3).

Gene ontology analysis revealed that the majority of proteins with differential abundance in response to IT surgery (and present in at least one depot) were associated with the following cellular components: cytoskeleton and remodeling of matrix, ribosomal, cytosolic, followed by intracellular, cell part, organelle (Figure 1). The broad cellular composition of fat depots [26,27] was confirmed by the differential expression of proteins, which — according to the protein databases — are expressed in platelets, red blood cells, macrophages, and muscle (Supplementary Dataset). Increases in proteins related to peripheral nervous system were detected in inguinal and epididymal as well as in mesenteric depots (Supplementary Dataset), whereas blood cells and vasculature-associated proteins were less abundant in response to IT surgery in all depots.

In terms of biological processes, the most significant differences were observed for proteins involved in glucose metabolism and glycerogenesis (Figure 1). The rest were part of muscle contraction, chromatin organization, blood circulation, mitosis, and organelle organization.

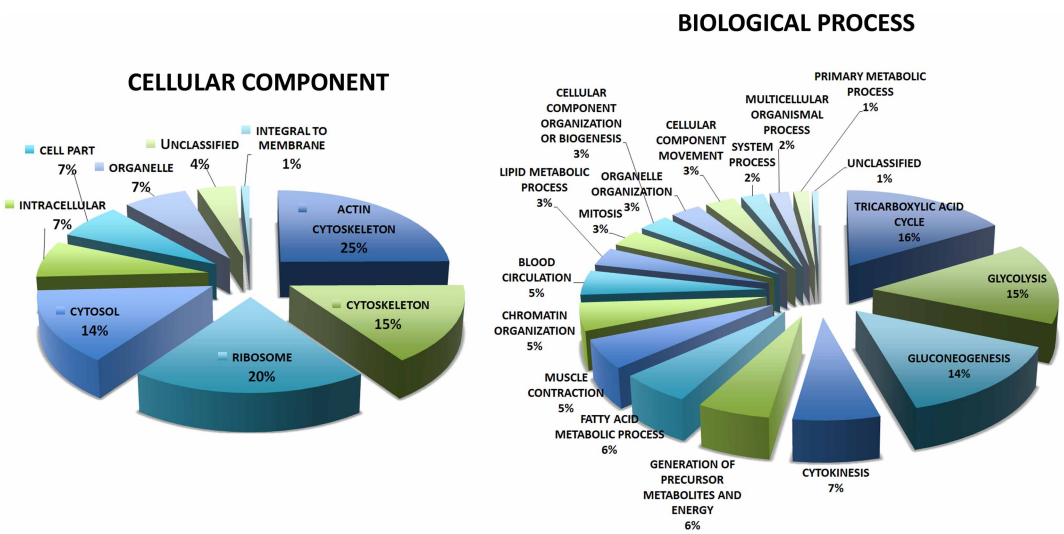

Figure 1. Gene ontology analysis of WAT proteome profiles at 1.5 m after IT surgery.

Gene ontology analysis (cellular component and biological process) was performed with the proteomic profile of all proteins that had different abundance between IT surgery ($n = 10$) and sham ($n = 9$) across all four depots in response to IT surgery, independent of the relative abundance of proteins (i.e. a protein showed higher abundance in response to IT surgery in one depot vs. lower abundance in another depot), and excluding those 'uncharacterized' (utilizing a seed of 363 from 377). All analyses were performed with proteins identified by mass spectrometry utilizing PANTHER.

Biochemical Journal (2018) **475** 649–662
https://doi.org/10.1042/BCJ20170899

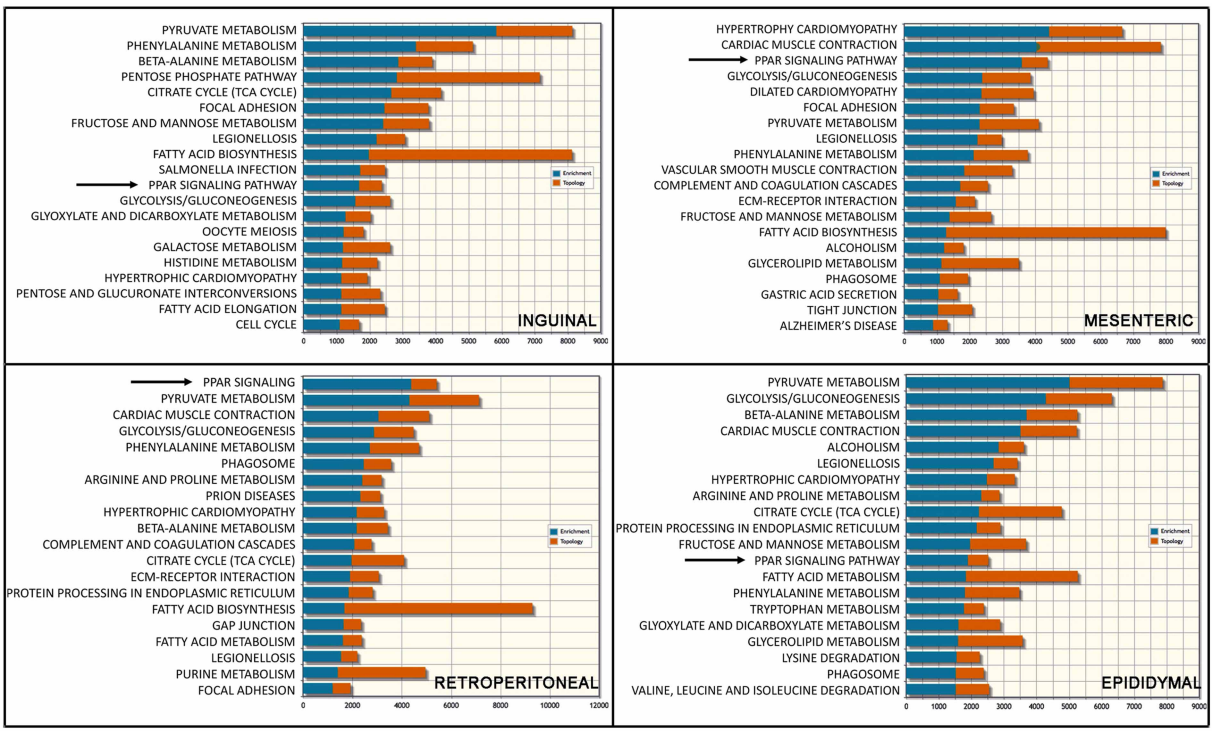

Figure 2. Pathway over-representation analyses of fat depots in response to IT surgery.

Pathway over-representation analyses were performed on each of the four fat depots ($n = 10$ IT and 9 sham animals) with the proteins differentially expressed as a consequence of the IT surgery. The analysis was performed by using MetaboAnalyst [24]. Enrichment analysis aimed at evaluating whether the observed proteins in a particular pathway were significantly enriched (appear more than expected by random chance) within the dataset. The over-representation analysis (ORA) was based on hypergeometrics analysis (shown in blue). The topology analysis (shown in orange) aimed at evaluating whether a given protein played an important role in response to the IT surgery based on its position within a pathway. The degree centrality measured the number of links that connected to a node (representing the protein) within a pathway.

Pathway over-representation and topology analyses indicated that IT surgery modified FFA metabolism (including elongation and glycerolipid metabolism) across all depots (Figure 2). Other pathways affected by the surgery were pentose phosphate, glycolysis, TCA (tricarboxylic acid) cycle, and hypertrophy. Interestingly, while the same pathways were affected in all four depots, when taking into account the fold change in protein abundance, those in mesenteric fat showed opposite trends than those in the other three depots (Figure 2).

IT surgery affects adipocyte differentiation and adipogenesis

Proteomics analysis showed overexpression of specific fatty acid transporters (Fabp4 and 5) and acyl-CoA-binding protein (Dbi), mainly in post-IT retroperitoneal, inguinal, and epididymal fats (Supplementary Dataset). Similarly, a significant number of enzymes involved in the uptake of glucose, glycolysis, and the TCA cycle were overall overexpressed in fat depots in response to IT surgery with the exception of the mesenteric depot (Supplementary Dataset). Finally, key enzymes in *de novo* lipogenesis (under 'Fatty acid biosynthesis', Supplementary Dataset) were overall over-represented in all depots, with the exception of mesenteric. Lipases that showed higher abundance were Ces1d in retroperitoneal and epididymal depots, Lipe in epididymal fat, and Ptrf in inguinal and epididymal fat depots (Supplementary Dataset). Pathway analysis indicated that after IT surgery relevant changes were associated with a significant number of lipid droplet (LD)-associated proteins, and important in the regulation of LD growth (i.e. SNAREs, motor proteins, cytoskeletal components, ribosomal proteins, proteasomal, lipid metabolism enzymes, signaling proteins, ER proteins, chaperones, and folding, among others; Supplementary Dataset under 'Cytoskeleton/EMC/dynamics'). Notably, depots other than inguinal and mesenteric exhibited the largest number of up-regulated cytoskeletal/matrix remodeling proteins (Supplementary Dataset). After IT surgery, a significant over-representation of proteins

Biochemical Journal (2018) **475** 649–662
https://doi.org/10.1042/BCJ20170899

related to cellular stress response was noted in all fat depots except the mesenteric (Supplementary Dataset under 'Antioxidant response'). Similarly, the expression of protein disulfide isomerases and peptidyl-prolyl *cis–trans* isomerases A (epididymal) and B (epididymal, retroperitoneal, and inguinal) were increased after IT surgery (Supplementary Dataset).

By selecting those proteins from Supplementary Dataset identified by the literature as being part of the adipocyte secretome during adipogenesis ([28]; Figure 3A), we distinguished those whose concentrations increased with the progression of adipogenesis (in the plain text), those that peaked at mid-process (in bold and italics), and those that declined from the onset of this process (in bold) (Figure 3A). Comparing the percentages of proteins that demonstrated higher vs. lower abundance after IT surgery for each depot (Figure 3B) as well as the average fold change (Figure 3C), it was evident that the secretome profile of epididymal fat was consistent with that of later stages of adipogenesis (ratio of high-over-low abundance of 3), whereas inguinal (ratio = 1.5) and retroperitoneal (ratio = 1.0) presented intermediate values. Conversely, the profile of mesenteric WAT appeared to closely resemble that of the pre-adipocyte stage.

In summary, based on the ratio of proteins with higher to lower abundance post-IT surgery, proteins associated with mature adipocytes (i.e. adipocyte maturation) seemed to be favored in epididymal, retroperitoneal, and inguinal depots, but not in mesenteric (Supplementary Dataset under 'Adipocyte differentiation' and 'Mature adipocytes').

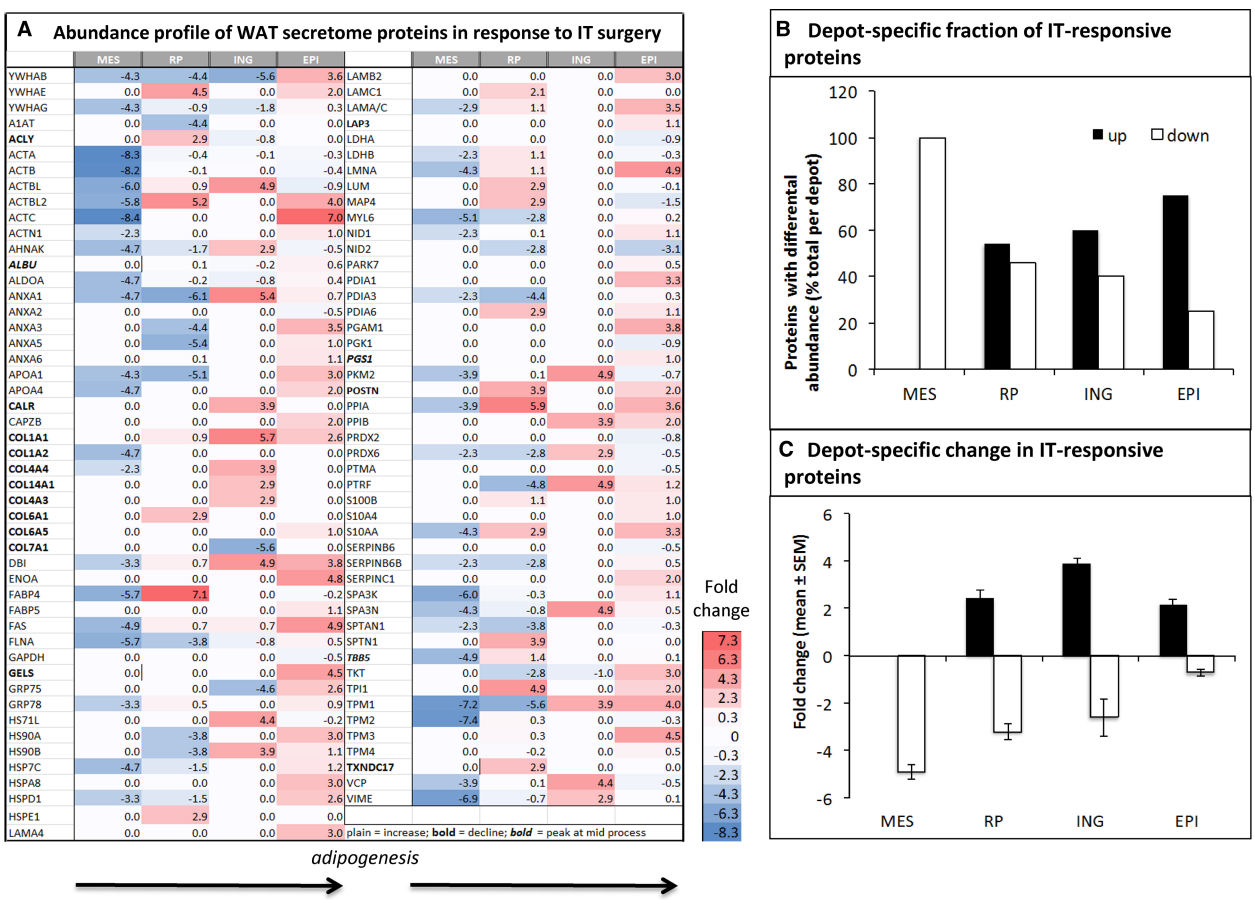

Figure 3. Effect of IT surgery on the WAT secretome profile in adipose depots.

(**A**) Proteins differentially expressed between IT ($n = 10$ animals) and sham ($n = 9$ animals) *per* depot were identified as being part of the adipocyte secretome during adipogenesis. Their abundance is shown as LOG2 ratio of IT/sham. Those proteins whose concentration increased with the progression of adipogenesis (shown in the plain text), those that peaked at mid-process (shown in bold and italics text), and those that declined from the onset of this process (in bold text). (**B**) Percentage of proteins per depot with a higher or lower abundance after IT surgery. (**C**) Average fold change for proteins under panel **B**.

Biochemical Journal (2018) **475** 649–662
https://doi.org/10.1042/BCJ20170899

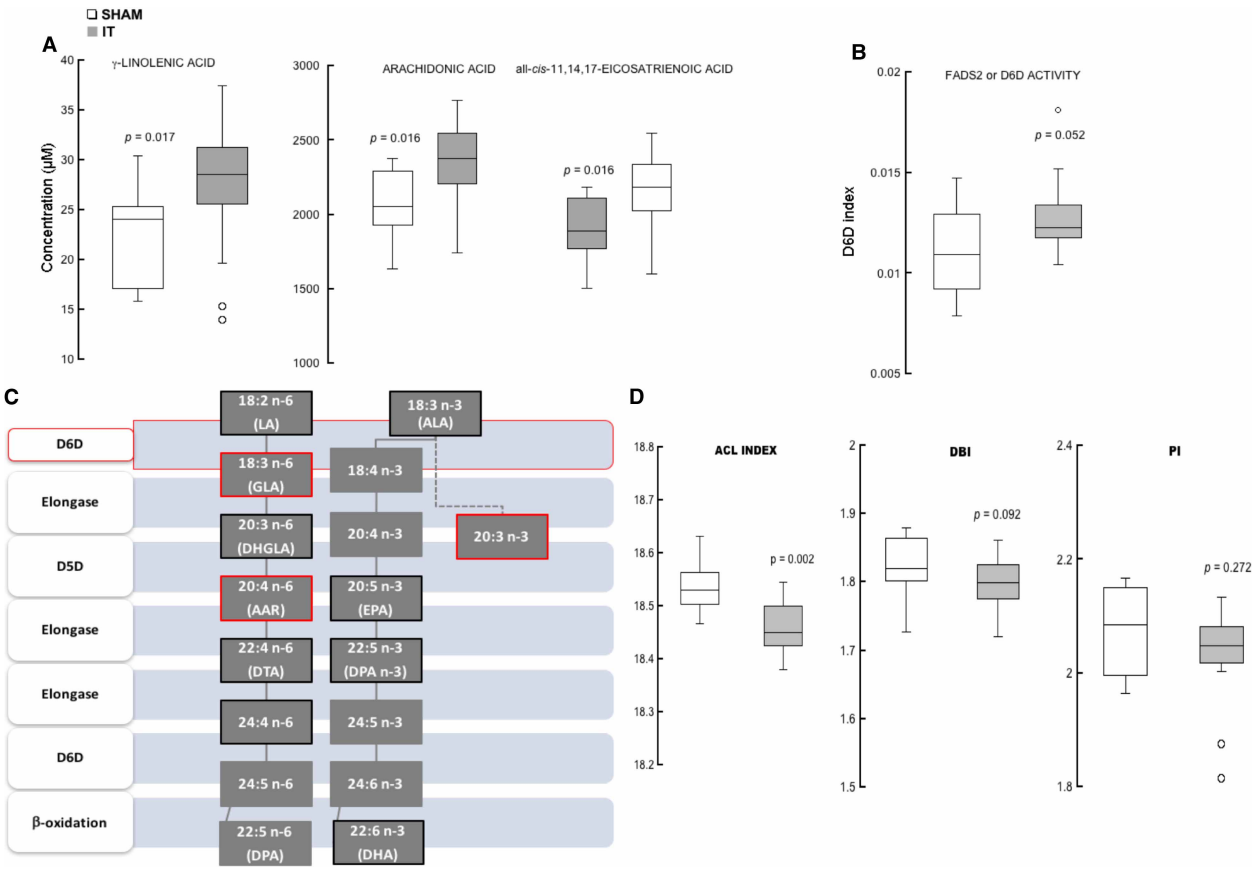

Figure 4. Plasma FFAs post-IT surgery and associated parameters.

(**A**) The profile of plasma FFA was performed in 13 sham and 12 IT animals at 1.5 m after IT or sham surgery. Only those fatty acids whose concentrations were significantly different are shown. (**B**) D6D index in sham and IT rats, calculated as indicated in the Materials and methods. (**C**) Conversion of linoleic and α-linolenic acid into longer-chain *n*-6 and *n*-3 PUFA by the action of D6D, D5D, and elongases. Boxes framed in black: compounds detected by FFA profile analysis; in red, higher concentration of compound in IT vs. sham. (**D**) ACL, DBI, and PI indices were calculated as indicated in the Materials and methods. Statistics were performed using the Student's *t*-test.

Increased adipocyte maturation through peroxisome proliferator-activated receptor gamma signaling

In terms of signaling, the peroxisome proliferator-activated receptor gamma (PPARγ) pathway emerged as a common mechanism across all depots in response to IT surgery (Figure 2) in line with the activation of this pathway during increased adipocyte maturation [29]. Indeed, several proteins known to be downstream targets of PPARγ (e.g. Fabp4, Fabp5, Dbi and Acsl1) showed higher abundance in IT vs. sham in all depots with the exception of mesenteric (Figure 3).

In an attempt to identify the possible activators of the PPARγ pathway as a result of IT surgery, and considering that FFAs are potent ligands of this factor [30], plasma FFA fatty acid composition was evaluated. Although plasma FFA profile may not reflect directly the metabolic status of adipose tissue, the only significant sites of FFA liberation into plasma are from adipose tissues with a plasma half-life of 2–4 min [31]. Plasma FFA profile revealed several important aspects related to PPARγ signaling pathway (Figure 4): (i) higher levels (15–20%) of three fatty acids [two *n*-6 polyunsaturated fat (PUFA) and one *n*-3 PUFA, eicosatrienoic acid (Figure 4A)] related to more pro-inflammatory states and adipocyte maturation and (ii) higher (15%) delta-6 desaturase (D6D) estimated activity in IT vs. sham (Figure 4B,C) with no differences for the estimated delta-5 desaturase (D5D) activity suggested increases in diabetes risk (not shown). (Of note, the use of fatty acid ratios as index of desaturase activity has been indicated as estimated because steady-state concentration ratios can be markers of altered incorporation, synthesis and/or secretion, or utilization [32]); (iii) no significant increases in

Biochemical Journal (2018) **475** 649–662
https://doi.org/10.1042/BCJ20170899

the resistance to lipid peroxidation was observed in IT based on the lack of differences in both the density of double bonds in FFA (double bond index or DBI) and the peroxidizability index (PI) (Figure 4D). The modest decrease in the average chain length (ACL) suggested some improvement in β-oxidation of FFA.

Taken together, the plasma FFA profile confirmed the proteomics and pathway analyses findings, as rats that underwent IT intervention compared with sham show pre-diabetic plasma biomarkers already at 1.5 m post-surgery.

Discussion

In a previous study, we reported that IT surgery in 4-month-old male UCD-T2DM rats delayed diabetes onset by an average of 120 days [6] which is equivalent to ∼10 years in humans [6,33]. In this study, to gain a deeper understanding of the molecular events underlying the effects of IT surgery, we examined the changes in the proteome of four WAT depots and plasma FFA profile in rats after 1.5 m of IT or sham surgery before they show overt signs of diabetes. Many rat models for type 2 diabetes (T2D) are available, including the Goto-Kakizaki (GK) (which represents a more suitable model for the study of T2D not associated with obesity [34]) and the Zucker Diabetic Fatty (ZDF) [35]. Compared with the ZDF rats, the UCD-T2DM model presents an obesity of polygenic origin, later onset of obesity, and T2DM, and a more moderate plasma TG elevation. Importantly, the UCD-T2DM model responds to the administration of exogenous leptin, leading to normalization of fasting glucose and lower HbA1c [36]. Other differences between the two models were presented in detail in a previous study from our group (see Table 5 in [11]).

Overall, the proteome profiles of these fat depots — except mesenteric — in response to IT surgery are consistent with a transition from pre-adipocyte to mature adipocyte differentiation. Conversely, the opposite trend observed in mesenteric fat seems to be consistent with the prevention or delay of the detrimental changes associated with adipocyte maturation, fat deposit and cell hypertrophy, and the ensuing development of T2DM. The major findings supporting these conclusions can be summarized as it follows: (a) IT surgery had a fat depot-specific effect mainly observed in the beneficial effect exerted on mesenteric fat; (b) the proteomic profile of mesenteric fat was consistent with a delayed adipocyte maturation compared with other depots with the involvement of cells other than adipocytes and the PPARγ pathway (Figure 5); (c) molecular markers of a pre-diabetic state are evidenced already at 1.5 m after IT surgery. Consistent with this last premise, others reported that certain biological processes (such as inflammation in the adipose tissue) precede the development of inflammation elsewhere and thus can act as early indicators for development and progression of disease in other tissues (e.g. β-cell failure and liver dysfunction; [37]).

Our results support the notion that the observed delayed onset of diabetes after IT surgery seems related to the decreased differentiation of adipocytes in a particular depot, mesenteric fat, and the only true visceral WAT evaluated, with increased remodeling of the neuroendocrine system. In this regard, recent studies point to the importance of LD-associated proteins and lipases in the dysregulation of adipocyte lipolysis in obesity [38]. The higher abundance of lipases (e.g. Ces1d, Lipe, and Ptrf) as well as other proteins important in the regulation of LD growth suggested that the adipocytes from fat depots other than mesenteric were at late stages of differentiation or with more mature adipocytes. In support of these findings, visceral adipocyte size was smaller and more prominent in mesenteric than subcutaneous adipose tissue [6], and this and our previous study showed decreases in the inflammatory/stress responses in mesenteric fat from UCD-T2DM rats 1.5 months after IT compared with sham [15]. In addition, the over-representation in a significant number of enzymes involved in the uptake of glucose, glycolysis, and the TCA cycle in fat depots in response to IT surgery (with the exception of the mesenteric depot) signals glucose uptake and metabolism as critical for mature adipocytes. The rate of glucose uptake into adipocytes is an important determinant of fat storage given that glycerol-3-phosphate is necessary for the glycerol backbone of triglyceride synthesis.

Interestingly, among the 13 most abundant proteins identified by our study in mesenteric fat following IT surgery, only one (insulinoma-associated protein 2; Insm2) has a clear role in diabetes [39]. Deletion of this gene in mice results in mild glucose intolerance and decreased glucose-responsive insulin secretion [40]. This protein is also present in the neurites of enteric neuronal cells, in the muscular layers of the stomach, small intestine, and colon, and it has been shown to be expressed in neuroendocrine cells that possess regulated secretory granules of neuropeptides and/or hormones [41]. Furthermore, two other proteins (i.e. Dlgp4 [42] and Arl8b [43]; Supplementary Dataset) of the 13 up-regulated in post-IT mesenteric fat are associated with synapsis maintenance and remodeling. Thus, it is likely that the presence of Insm2 in mesenteric WAT may favor the formation of secretory vesicles with neuropeptides or adipokines affecting other organs, especially the

Biochemical Journal (2018) **475** 649–662
https://doi.org/10.1042/BCJ20170899

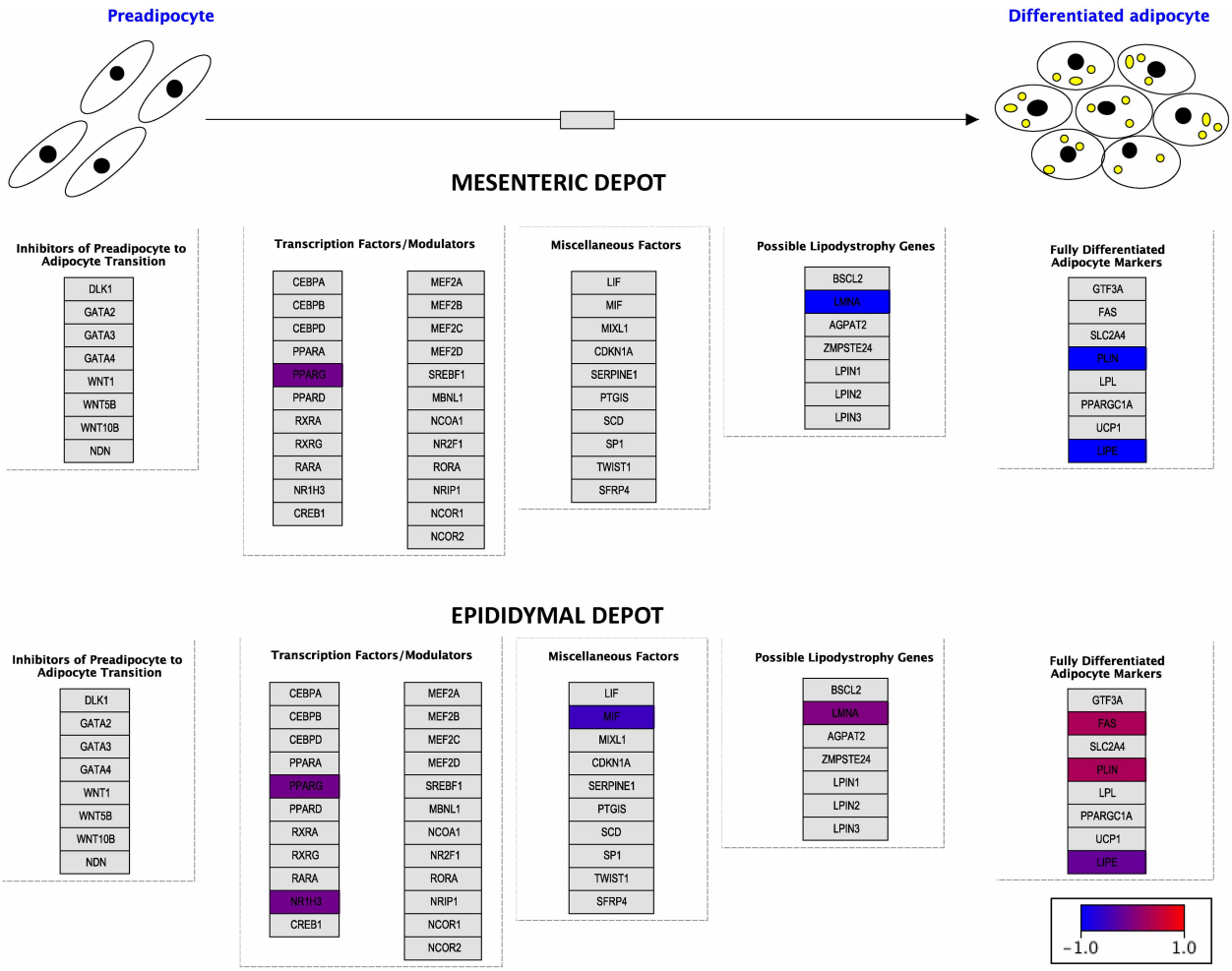

Figure 5. Differential expression of key proteins in adipocyte maturation in response to IT surgery.

Differences in protein expression patterns between mesenteric (IT/sham; $n = 10$ IT and 9 sham) and epididymal (IT/sham; $n = 10$ IT and 9 sham) depots in the context of adipocyte maturation. Epididymal was taken as a representative of the non-mesenteric depots' protein expression profiles. Scheme was built with the PathVisio software.

liver. Alternatively, heightening the neuroendocrine system in mesenteric fat may reduce the differentiation of mesenchymal stem cells to adipocytes [44] or promote pre-adipocyte proliferation but not their differentiation [45]. Indeed, an increased number of enteroendocrine cells were observed in the intestine of rats that underwent IT surgery [46].

Of relevance, ER stress is known to play an important role in obesity, insulin resistance, and T2DM, but, more recently, as an inhibitor of adipocyte differentiation [47]. Intriguingly, the significant over-representation of proteins related to cellular stress response including unfolded protein response after IT surgery noted in all fat depots, except that the mesenteric may represent an attempt to fight increased cellular stress and sustain the maturation process. Indeed, our previous report showed that IT-operated rats had decreased activation of Perk, Atf6, Ire1, and Grp78/BiP in the liver, skeletal muscle, pancreas, and adipose tissue, suggesting that IT surgery decreased ER stress at 1.5 months post-surgery in UCD-T2DM rats [15]. Increased ER stress can also lead to misfolding or unfolding in proteins, which stimulates a response known as the unfolded protein response, mediated by ER membrane-associated proteins [7].

Given the variety of pathways over-represented by the tissue proteomics, it is important to note that mature adipocytes constitute ~50% of the total cell content of most fat depots, with the rest being constituted by pre-adipocytes, endothelial cells, macrophages, and mast and dendritic cells, sympathetic and sensory nerve fibers,

Biochemical Journal (2018) **475** 649–662
https://doi.org/10.1042/BCJ20170899

as well as stem cells [48]. In this regard, none of the responses by WAT depots were necessarily linked to the fat or protein mass. Assuming that the adipocyte number is proportional to the fat content, then subcutaneous fat has the highest adipocyte-to-non-adipocyte ratio (in contrast with visceral adipose tissue). This indicates that some of the responses observed for mesenteric fat were mediated by cells other than adipocytes modulating adipocyte fate in a bi-directional neuron–adipocyte cross-talk.

Pathway analysis highlighted the involvement of the PPARγ pathway (down-regulated in mesenteric with opposite responses in the rest of the depots), possibly modulated by the *n*-6/*n*-3 FFA ratio. The higher plasma *n*-6/*n*-3 ratio is indicative of increased adipocyte proliferation and differentiation, lipogenesis and PPARγ signaling [49], as well as a more pro-inflammatory state. As eicosanoid levels derived from the *n*-3 and *n*-6 series are controlled by the rate-limiting steps catalyzed by D5D and D6D [50], the higher D6D index was also consistent with a pre-diabetic state because this activity correlates directly with diabetes risk and insulin resistance (whereas D5D activity has a reciprocal correlation; [51]) and with inflammatory marker IL-1β in both visceral and subcutaneous fat [23]. If this scenario is correct, the proteomics of non-visceral fat depots align more closely to the plasma FFA profile. Then, the role of non-visceral fats could be more ascribed at providing readily available sources of fuel and paracrine factors to neighboring tissues [52]. In contrast, IT surgery, a process that favors the delivery of incompletely digested nutrients, bile acids and salts, and pancreatic enzymes to the ileum [2], affects mainly a fat depot (mesenteric) more anatomically associated with the intestine (organ cross-talk; [10]).

Previous studies proposed that another contributing factor of improved lipid metabolism after IT surgery may be attributed to increased levels of total circulating bile acids, and in particular, a higher proportion of non-conjugated cholic acid [6,15]. In those studies, it was proposed that increases in cholic acid levels modulate ER stress contributing to improved insulin sensitivity and preservation of β-cell mass. However, proteomic analyses revealed only one protein connected with bile acid metabolism (NR1H4; Supplementary Dataset) with lower abundance in post-IT retroperitoneal fat depot. Then, IT surgery may be enhancing not only the absorption of bile acids but also that of FFA possibly resulting in a higher uptake of those of the *n*-3 over the *n*-6 series, which would promote the inhibition of adipocyte differentiation in this depot via PPARγ signaling.

Consistent with our results indicating mesenteric fat as one of the main targets of the delayed diabetes onset in response to IT surgery, visceral adiposity is associated with chronic low-grade inflammation, which promotes adipocyte dysfunction, insulin resistance, and β-cell damage. In studies using magnetic resonance imaging and computed tomography, increased visceral fat mass was specifically related to insulin resistance [53], and surgical removal of visceral fat in rodent models of type-2 diabetes also improved hepatic insulin sensitivity and glucose tolerance while reducing gluconeogenesis [54].

Our study has some limitations, i.e. the use of combined samples for proteomics which eliminates the inter-individual variations, the use of protein expression as a marker for activities within pathways minimizing metabolite-driven and epigenetic effects, and the evaluation of fat depot metabolism at time points shorter than at 1.5-m post-IT surgery to evaluate earlier metabolic changes. Nevertheless, our findings suggest that the use of surgical strategies that seek diabetes onset delay and/or symptoms improvements should contemplate the involvement of adipose depot-specific effect assessment in diabetes prevention and/or remission, paying special attention to early, molecular predictors of pre-diabetic states, and how to manipulate these responses to implement a long-lasting, post-surgery beneficial impact.

Abbreviations

ACL, average chain length; D5D, delta-5 desaturase; D6D, delta-6 desaturase; DBI, double bond index; ER, endoplasmic reticulum; FFA, free fatty acids; GLP-1, glucagon-like peptide-1; Hb, hemoglobin; Insm2, insulinoma-associated protein 2; IT, ileal interposition; LD, lipid droplets; MS, mass spectrometry; PI, peroxidizability index; PPARγ, peroxisome proliferator-activated receptor gamma; PUFA, polyunsaturated fats; T2D, type 2 diabetes; T2DM, type 2 diabetes mellitus; TCA, tricarboxylic acid; TG, triglycerides; WAT, white adipose tissue.

Author Contribution

C.H. and C.B. prepared all samples for mass spectrometry analysis. E.N. helped drafting and edited the manuscript and figures. J.G. collected data for Table 1 and Table 2 and free fatty acid profile. K.L.S., I.M., and M.C.G. revised/edited the manuscript. P.J.H. provided the tissues utilized in the present study, supervised the data collected under Table 1 and Table 2, and edited the manuscript. C.G. conceptualized the study, designed the experiments, analyzed the data, and wrote the manuscript.

Funding

The present study was funded by National Institute of Diabetes and Digestive and Kidney Diseases (NIDDK) RC1 DK087307.

Acknowledgements

We thank Dr Bethany Cummings for performing all of the surgeries.

Competing Interests

The Authors declare that there are no competing interests associated with the manuscript information.

References

1 Menon, K., Mousa, A., de Courten, M.P., Soldatos, G., Egger, G. and de Courten, B. (2017) Shared medical appointments may be effective for improving clinical and behavioral outcomes in type 2 diabetes: a narrative review. *Front. Endocrinol.* **8**, 263 https://doi.org/10.3389/fendo.2017.00263

2 Chelikani, P.K., Shah, I.H., Taqi, E., Sigalet, D.L. and Koopmans, H.H. (2010) Comparison of the effects of Roux-en-Y gastric bypass and ileal transposition surgeries on food intake, body weight, and circulating peptide YY concentrations in rats. *Obes. Surg.* **20**, 1281–1288 https://doi.org/10.1007/s11695-010-0139-6

3 Thaler, J.P. and Cummings, D.E. (2009) Minireview: hormonal and metabolic mechanisms of diabetes remission after gastrointestinal surgery. *Endocrinology* **150**, 2518–2525 https://doi.org/10.1210/en.2009-0367

4 Wickremesekera, K., Miller, G., Naotunne, T.D., Knowles, G. and Stubbs, R.S. (2005) Loss of insulin resistance after Roux-en-Y gastric bypass surgery: a time course study. *Obes. Surg.* **15**, 474–481 https://doi.org/10.1381/0960892053723402

5 Schauer, P.R., Burguera, B., Ikramuddin, S., Cottam, D., Gourash, W., Hamad, G. et al. (2003) Effect of laparoscopic Roux-en Y gastric bypass on type 2 diabetes mellitus. *Ann. Surg.* **238**, 467–484; discussion 484–465 https://doi.org/10.1097/01.sla.0000089851.41115.1b

6 Cummings, B.P., Strader, A.D., Stanhope, K.L., Graham, J.L., Lee, J., Raybould, H.E. et al. (2010) Ileal interposition surgery improves glucose and lipid metabolism and delays diabetes onset in the UCD-T2DM rat. *Gastroenterology.* **138**, 2437–2446; 2446 e2431 https://doi.org/10.1053/j.gastro.2010.03.005

7 Su, J., Zhou, L., Kong, X., Yang, X., Xiang, X., Zhang, Y. et al. (2013) Endoplasmic reticulum is at the crossroads of autophagy, inflammation, and apoptosis signaling pathways and participates in the pathogenesis of diabetes mellitus. *J. Diabetes Res.* **2013**, 193461 https://doi.org/10.1155/2013/193461

8 Einstein, F.H., Atzmon, G., Yang, X.M., Ma, X.H., Rincon, M., Rudin, E. et al. (2005) Differential responses of visceral and subcutaneous fat depots to nutrients. *Diabetes* **54**, 672–678 https://doi.org/10.2337/diabetes.54.3.672

9 Hamdy, O., Porramatikul, S. and Al-Ozairi, E. (2006) Metabolic obesity: the paradox between visceral and subcutaneous fat. *Curr. Diab. Rev.* **2**, 367–373 https://doi.org/10.2174/1573399810602040367

10 Bjorntorp, P. (1990) "Portal" adipose tissue as a generator of risk factors for cardiovascular disease and diabetes. *Arteriosclerosis* **10**, 493–496 https://doi.org/10.1161/01.ATV.10.4.493

11 Cummings, B.P., Digitale, E.K., Stanhope, K.L., Graham, J.L., Baskin, D.G., Reed, B.J. et al. (2008) Development and characterization of a novel rat model of type 2 diabetes mellitus: the UC Davis type 2 diabetes mellitus UCD-T2DM rat. *Am. J. Physiol. Regul. Integr. Comp. Physiol.* **295**, R1782–R1793 https://doi.org/10.1152/ajpregu.90635.2008

12 Basu, U., Romao, J.M. and Guan le, L. (2013) Adipogenic transcriptome profiling using high throughput technologies. *J. Genomics.* **1**, 22–28 https://doi.org/10.7150/jgen.3781

13 Romao, J.M., Jin, W., He, M., McAllister, T. and Guan, L.L. (2013) Elucidation of molecular mechanisms of physiological variations between bovine subcutaneous and visceral fat depots under different nutritional regimes. *PLoS ONE* **8**, e83211 https://doi.org/10.1371/journal.pone.0083211

14 Gry, M., Rimini, R., Stromberg, S., Asplund, A., Ponten, F., Uhlen, M. et al. (2009) Correlations between RNA and protein expression profiles in 23 human cell lines. *BMC Genomics* **10**, 365 https://doi.org/10.1186/1471-2164-10-365

15 Cummings, B.P., Bettaieb, A., Graham, J.L., Kim, J., Ma, F., Shibata, N. et al. (2013) Bile-acid-mediated decrease in endoplasmic reticulum stress: a potential contributor to the metabolic benefits of ileal interposition surgery in UCD-T2DM rats. *Dis. Model Mech.* **6**, 443–456 https://doi.org/10.1242/dmm.010421

16 Ross-Inta, C.M., Zhang, Y.F., Almendares, A. and Giulivi, C. (2009) Threonine-deficient diets induced changes in hepatic bioenergetics. *Am. J. Physiol. Gastrointest. Liver Physiol.* **296**, G1130–G1139 https://doi.org/10.1152/ajpgi.90545.2008

17 Chen, H.C. and Farese, Jr, R.V. (2002) Determination of adipocyte size by computer image analysis. *J. Lipid Res.* **43**, 986–989 PMID:12032175

18 Napoli, E., Ross-Inta, C., Song, G., Wong, S., Hagerman, R., Gane, L.W. et al. (2016) Premutation in the fragile X mental retardation 1 (FMR1) gene affects maternal Zn-milk and perinatal brain bioenergetics and scaffolding. *Front. Neurosci.* **10**, 159 https://doi.org/10.3389/fnins.2016.00159

19 Keller, A., Nesvizhskii, A.I., Kolker, E. and Aebersold, R. (2002) Empirical statistical model to estimate the accuracy of peptide identifications made by MS/MS and database search. *Anal. Chem.* **74**, 5383–5392 https://doi.org/10.1021/ac025747h

20 Nesvizhskii, A.I., Keller, A., Kolker, E. and Aebersold, R. (2003) A statistical model for identifying proteins by tandem mass spectrometry. *Anal. Chem.* **75**, 4646–4658 https://doi.org/10.1021/ac0341261

21 Fiehn, O. (2008) Extending the breadth of metabolite profiling by gas chromatography coupled to mass spectrometry. *Trends Analyt. Chem.* **27**, 261–269 https://doi.org/10.1016/j.trac.2008.01.007

22 Jove, M., Naudi, A., Aledo, J.C., Cabre, R., Ayala, V., Portero-Otin, M. et al. (2013) Plasma long-chain free fatty acids predict mammalian longevity. *Sci. Rep.* **3**, 3346 https://doi.org/10.1038/srep03346

23 Vaittinen, M., Walle, P., Kuosmanen, E., Mannisto, V., Kakela, P., Agren, J. et al. (2016) *FADS2* genotype regulates delta-6 desaturase activity and inflammation in human adipose tissue. *J. Lipid Res.* **57**, 56–65 https://doi.org/10.1194/jlr.M059113

24 Xia, J. and Wishart, D.S. (2016) Using MetaboAnalyst 3.0 for comprehensive metabolomics data analysis. *Curr. Protoc. Bioinformatics.* **55**, 14 10 11–14 10 91 https://doi.org/10.1002/cpbi.11

Biochemical Journal (2018) **475** 649–662
https://doi.org/10.1042/BCJ20170899

25 Baggio, L.L. and Drucker, D.J. (2007) Biology of incretins: GLP-1 and GIP. *Gastroenterology* **132**, 2131–2157 https://doi.org/10.1053/j.gastro.2007.03.054
26 Peinado, J.R., Jimenez-Gomez, Y., Pulido, M.R., Ortega-Bellido, M., Diaz-Lopez, C., Padillo, F.J. et al. (2010) The stromal-vascular fraction of adipose tissue contributes to major differences between subcutaneous and visceral fat depots. *Proteomics* **10**, 3356–3366 https://doi.org/10.1002/pmic.201000350
27 Peinado, J.R., Pardo, M., de la Rosa, O. and Malagón, M.M. (2012) Proteomic characterization of adipose tissue constituents, a necessary step for understanding adipose tissue complexity. *Proteomics* **12**, 607–620 https://doi.org/10.1002/pmic.201100355
28 Zhong, J., Krawczyk, S.A., Chaerkady, R., Huang, H., Goel, R., Bader, J.S. et al. (2010) Temporal profiling of the secretome during adipogenesis in humans. *J. Proteome Res.* **9**, 5228–5238 https://doi.org/10.1021/pr100521c
29 Moseti, D., Regassa, A., and Kim, W.K. (2016) Molecular regulation of adipogenesis and potential anti-adipogenic bioactive molecules. *Int. J. Mol. Sci.* **17**, 124 https://doi.org/10.3390/ijms17010124
30 Ahmadian, M., Suh, J.M., Hah, N., Liddle, C., Atkins, A.R., Downes, M. et al. (2013) PPARγ signaling and metabolism: the good, the bad and the future. *Nat. Med.* **99**, 557–566 https://doi.org/10.1038/nm.3159
31 Karpe, F., Dickmann, J.R. and Frayn, K.N. (2011) Fatty acids, obesity, and insulin resistance: time for a reevaluation. *Diabetes* **60**, 2441–2449 https://doi.org/10.2337/db11-0425
32 Brown, J.E., Lindsay, R.M. and Riemersma, R.A. (2000) Linoleic acid metabolism in the spontaneously diabetic rat: Δ6-desaturase activity vs. product/precursor ratios. *Lipids* **35**, 1319–1323 https://doi.org/10.1007/s11745-000-0648-1
33 Sengupta, P. (2013) The laboratory rat: relating its age with human's. *Int. J. Prev. Med.* **4**, 624–630 PMID:23930179
34 Portha, B., Giroix, M.H., Tourrel-Cuzin, C., Le-Stunff, H. and Movassat, J. (2012) The GK rat: a prototype for the study of non-overweight type 2 diabetes. *Methods Mol. Biol.* **933**, 125–159 https://doi.org/10.1007/978-1-62703-068-7_9
35 Siwy, J., Zoja, C., Klein, J., Benigni, A., Mullen, W., Mayer, B. et al. (2012) Evaluation of the Zucker diabetic fatty (ZDF) rat as a model for human disease based on urinary peptidomic profiles. *PLoS ONE* **7**, e51334 https://doi.org/10.1371/journal.pone.0051334
36 Cummings, B.P., Bettaieb, A., Graham, J.L., Stanhope, K.L., Dill, R., Morton, G.J. et al. (2011) Subcutaneous administration of leptin normalizes fasting plasma glucose in obese type 2 diabetic UCD-T2DM rats. *Proc. Natl Acad. Sci. U.S.A.* **108**, 14670–14675 https://doi.org/10.1073/pnas.1107163108
37 Mori, M.A., Liu, M., Bezy, O., Almind, K., Shapiro, H., Kasif, S. et al. (2010) A systems biology approach identifies inflammatory abnormalities between mouse strains prior to development of metabolic disease. *Diabetes* **59**, 2960–2971 https://doi.org/10.2337/db10-0367
38 Brasaemle, D.L. (2007) *Thematic review series: adipocyte biology.* The perilipin family of structural lipid droplet proteins: stabilization of lipid droplets and control of lipolysis. *J. Lipid. Res.* **48**, 2547–2559 https://doi.org/10.1194/jlr.R700014-JLR200
39 Nakajima, K., Wu, G., Takeyama, N., Sakudo, A., Sugiura, K., Yukawa, M. et al. (2009) Insulinoma-associated protein 2-deficient mice develop severe forms of diabetes induced by multiple low doses of streptozotocin. *Int. J. Mol. Med.* **24**, 23–27 https://doi.org/10.3892/ijmm_00000201
40 Kubosaki, A., Gross, S., Miura, J., Saeki, K., Zhu, M., Nakamura, S. et al. (2004) Targeted disruption of the IA-2β gene causes glucose intolerance and impairs insulin secretion but does not prevent the development of diabetes in NOD mice. *Diabetes* **53**, 1684–1691 https://doi.org/10.2337/diabetes.53.7.1684
41 Takeyama, N., Ano, Y., Wu, G., Kubota, N., Saeki, K., Sakudo, A. et al. (2009) Localization of insulinoma associated protein 2, IA-2 in mouse neuroendocrine tissues using two novel monoclonal antibodies. *Life Sci.* **84**, 678–687 https://doi.org/10.1016/j.lfs.2009.02.012
42 Kim, Y., Zhang, Y., Pang, K., Kang, H., Park, H., Lee, Y. et al. (2016) Bipolar disorder associated microRNA, miR-1908-5p, regulates the expression of genes functioning in neuronal glutamatergic synapses. *Exp. Neurobiol.* **25**, 296–306 https://doi.org/10.5607/en.2016.25.6.296
43 Haraguchi, T., Yanaka, N., Nogusa, Y., Sumiyoshi, N., Eguchi, Y. and Kato, N. (2006) Expression of ADP-ribosylation factor-like protein 8B mRNA in the brain is down-regulated in mice fed a high-fat diet. *Biosci. Biotechnol. Biochem.* **70**, 1798–1802 https://doi.org/10.1271/bbb.60168
44 Lee, Y.Y., Moujalled, D., Doerflinger, M., Gangoda, L., Weston, R., Rahimi, A. et al. (2013) CREB-binding protein (CBP) regulates β-adrenoceptor (β-AR)-mediated apoptosis. *Cell Death Differ.* **20**, 941–952 https://doi.org/10.1038/cdd.2013.29
45 Collins, S. (2011) β-Adrenoceptor signaling networks in adipocytes for recruiting stored fat and energy expenditure. *Front. Endocrinol.* **2**, 102 https://doi.org/10.3389/fendo.2011.00102
46 Hansen, C.F., Vassiliadis, E., Vrang, N., Sangild, P.T., Cummings, B.P., Havel, P. et al. (2014) The effect of ileal interposition surgery on enteroendocrine cell numbers in the UC Davis type 2 diabetes mellitus rat. *Regul. Pept.* **189**, 31–39 https://doi.org/10.1016/j.regpep.2014.01.002
47 Longo, M., Spinelli, R., D'Esposito, V., Zatterale, F., Fiory, F., Nigro, C. et al. (2016) Pathologic endoplasmic reticulum stress induced by glucotoxic insults inhibits adipocyte differentiation and induces an inflammatory phenotype. *Biochim. Biophys. Acta* **1863**, 1146–1156 https://doi.org/10.1016/j.bbamcr.2016.02.019
48 Trayhurn, P., Drevon, C.A. and Eckel, J. (2011) Secreted proteins from adipose tissue and skeletal muscle — adipokines, myokines and adipose/muscle cross-talk. *Arch. Physiol. Biochem.* **117**, 47–56 https://doi.org/10.3109/13813455.2010.535835
49 An, L., Pang, Y.W., Gao, H.M., Tao, L., Miao, K., Wu, Z.H. et al. (2012) Heterologous expression of *C. elegans* fat-1 decreases the n-6/n-3 fatty acid ratio and inhibits adipogenesis in 3T3-L1 cells. *Biochem. Biophys. Res. Commun.* **428**, 405–410 https://doi.org/10.1016/j.bbrc.2012.10.068
50 Martinelli, N., Girelli, D., Malerba, G., Guarini, P., Illig, T., Trabetti, E. et al. (2008) FADS genotypes and desaturase activity estimated by the ratio of arachidonic acid to linoleic acid are associated with inflammation and coronary artery disease. *Am. J. Clin. Nutr.* **88**, 941–949 PMID:18842780
51 Kröger, J. and Schulze, M.B. (2012) Recent insights into the relation of Δ5 desaturase and Δ6 desaturase activity to the development of type 2 diabetes. *Curr. Opin. Lipidol.* **23**, 4–10 https://doi.org/10.1097/MOL.0b013e32834d2dc5
52 Caesar, R., Manieri, M., Kelder, T., Boekschoten, M., Evelo, C., Muller, M. et al. (2010) A combined transcriptomics and lipidomics analysis of subcutaneous, epididymal and mesenteric adipose tissue reveals marked functional differences. *PLoS ONE* **5**, e11525 https://doi.org/10.1371/journal.pone.0011525
53 Despres, J.P., Lemieux, S., Lamarche, B., Prud'homme, D., Moorjani, S., Brun, L.D. et al. (1995) The insulin resistance-dyslipidemic syndrome: contribution of visceral obesity and therapeutic implications. *Int. J. Obes. Relat. Metab. Disord.* **19** (Suppl 1), S76–S86 PMID:7550542
54 Miyazaki, Y., Pipek, R., Mandarino, L.J. and DeFronzo, R.A. (2003) Tumor necrosis factor α and insulin resistance in obese type 2 diabetic patients. *Int. J. Obes. Relat. Metab. Disord.* **27**, 88–94 https://doi.org/10.1038/sj.ijo.0802187